Parent material and climate interact to control soil C dynamics through the development of poorly crystalline minerals

Jeffrey Beem-Miller[1], Craig Rasmussen[2], Alison M. Hoyt[1,3], Marion Schrumpf[1], Georg Guggenberger[4], & Susan Trumbore[1]

[1] Department of Biogeochemical Processes, Max Planck Institute for Biogeochemistry, Jena, Germany

[2] Department of Environmental Science, The University of Arizona, Tucson, AZ, USA

[3] Department of Earth System Science Science, Stanford University, Stanford, CA, USA

[4] Institute of Soil Science, Leibniz University Hannover, Hannover, Germany

Abstract

Lorem ipsum...

Parent material and climate interact to control soil C dynamics through the development of poorly crystalline minerals

Key messages:

- Climate explains more variance in $\Delta^{14}C$ at the soil surface; parent material explains more variance at depth
- Interaction of parent material and climate explains more variance in bulk soil and respired $\Delta^{14}C$ than either factor alone
- Poorly crystalline mineral content is highly correlated with the difference between bulk soil $\Delta^{14}C$ and respired $\Delta^{14}C_{respired}$

Introduction

- Climate change effects on soil C will determine whether or not soils continue to be a sink or will become a source in the coming decades
  - Understanding these effects requires understanding soil carbon persistence mechanisms
  - This study specifically looking at parent material, climate, and their interaction via weathering
- Climate most important explanatory factor for global variation in C stocks and $\Delta^{14}C$
  - Function of temperature and moisture effect on decomposition rates
- Mineral association attenuates these effects
  - Examples of decomposition rates different for different parent materials under the same climate conditions
  - Lab and field?
  - E.g. . . .
- Mechanisms of mineral protection and specific minerals, i.e. beyond clay

- Poorly crystalline minerals in particular
- Develop from interaction of parent material and climate over time, i.e. weathering
- Examples of mechanisms

- Bulk soil $\Delta^{14}C$ as proxy for age
  - Larger pools that cycle more slowly dominate mass of bulk soil C, but contribute less to respired C fluxes
  - $\Delta^{14}C$ of heterotrophically respired CO_2 ($\Delta^{14}C_{respired}$) gives relative contribution of faster or more slowly cycling soil C to flux
  - $\Delta^{14}C_{respired}$ emphasizes contributions from smaller, fast cycling pools
  - Therefore difference between two provides a measure of the degree of protection of soil C (or presence of C pools that are persistent over centuries-millennnia because of strong mineral protection)
- Introduce sites
  - ...
- Expectations for effects of parent material and climate effects
  - Linear models (?)
  - Teaser of findings, importance of weathering for mineral assemblage;
  - Interaction of parent material and climate key for understanding the variance in $\Delta^{14}C$ of both bulk soil and respired CO_2
  - Show how poorly crystalline minerals implicated in soil C protection

Methods

Site descriptions

We collected samples from 9 sites across a combined gradient of parent material and climate in the Sierra Nevada Mountains of California (Table 1). These mountains provide natural independent gradients of parent material and mean annual temperature (MAT).

Moving from north to south along the cordillera the parent material changes from basalt to andesite to granite, while the change in elevation headed eastward from the Central Valley leads to a decrease in MAT that is consistent for each parent material.

Total mean annual precipitation is relatively constant with elevation, but falls mainly as rain at lower elevations, and mainly as snow at higher elevations. There is a slight precipitation gradient running north to south, with MAP of xxx mm yr^{-1} averaged across the basalt sites in the north, xxx mm yr-1 for the andesitic sites, and xxx mm yr^{-1} for the granodiorite sites in the south.

Vegetation at the study sites is typical of the Sierra Mixed Conifer habitat (Parker, I., and W. J. Matyas. 1981. CALVEG: a classification of Californian vegetation. U.S. Dep. Agric., For. Serv., Reg. Ecol. Group, San Francisco.). All of the sites are forested and dominated by conifers, although the species composition changes along with climate. Tree species at the lowest elevation, "warm", sites are predominantly Pinus ponderosa mixed with lesser amounts of Quercus spp. The canopy species at the mid-elevation cool sites is comprised primarily of Abies concolor and Pinus lambertiana, while Abies magnifica is the dominant species at the highest elevation "cold" sites. Species present at all sites include Calocedrus decurrens in the canopy, the shrubs Arctostaphylos spp., Chamaebatia foliolosa, and Ceanothus spp. to varying degrees, and ground cover of grasses and forbs.

Sample collection

Site locations were initially established in 2001 by C. Rasmussen (Rasmussen et al., 2006), and resampled in 2009 (Rasmussen et al., 2018). We returned in late September of 2019 to collect samples for this study. Sites were located using GPS and geospatial coordinates recorded during site establishment. At each site we dug three replicate pits down to a depth of 0.3m. Prior to sample collection we compared the soil profiles to the pedon

descriptions from the previous sampling campaigns. After confirming profiles were comparable we collected samples from the pit sidewalls in 0.1m increments for each of the three pits. We also measured the depth of the litter layer and collected representative litter samples from each site.

Spline fitting

Soils collected in 2001 and 2009 were sampled by horizon, while soils collected in 2019 were sampled by depth. We were motivated to use consistent depth increments across sites because of the strong correlation between depth and $\Delta^{14}C$ In order to make the horizon and depth-based measurements comparable, we fit a mass-preserving quadratic spline to the 2001 and 2009 profiles in order to convert soil property data to the equivalent depth increments sampled in 2019 (Bishop et al., 2001). We used the mpspline function of the GSIF package in R, with a lamba value of 0.1 (Hengl 2019).

Incubations

Laboratory soil incubations were performed on composite samples from the three replicate pedons sampled at each site. We composited and incubated each depth increment (0-10cm, 10-20cm, 20-30cm) separately in 1 L glass mason jars fitted with sampling ports in the lids. Incubations were performed in duplicate. Prior to the start of incubations we adjusted the soil moisture content to 60% of water holding capacity (WHC). We defined WHC as the gravimetric water content of water-saturated soil placed in mesh-covered (50µm) tubes (50ml) weighed after draining for 30 minutes on a bed of fine sand. Following rewetting we allowed the soils to respire for one week before closing the jars. Incubations proceeded until CO_2 concentrations in the jar headspace reached approximately 10,000 ppm, at which point we collected a 400ml gas subsample for radicocarbon analysis. Gas samples

were collected with pre-evacuated stainless-steel (Restec) vacuum canisters. All incubations were performed in the dark at 20°C.

Soil Physical Analyses and Mineral Characterization

Data on soil particle size distributions, bulk density, and mineral characterization were obtained from previously published analyses of samples collected at the study sites in 2001 and 2009 (Rasmussen et al. 2006, Rasmussen et al., 2018). Both qualitative and quantitative approaches were used to characterize soil mineral assemblages, including X-ray diffraction (XRD) for the clay (<2µm) fraction, atomic absorption spectroscopy, and non-sequential selective dissolution. Details on these analyses are provided by Rasmussen et al. (20XX). In this study we use the amount of iron selectively dissolved from bulk soils by acid ammonium-oxalate and citrate dithionite as proxies for the quantity of poorly crystalline and crystalline minerals, respectively.

Carbon, Nitrogen, and Radiocarbon Analysis

Total carbon and nitrogen content was determined by dry combustion (Vario Max, Elementar Analysensysteme GmbH) on finely ground soils (Retch MM400). For radiocarbon analysis, we first purified CO_2 from incubation flask samples and combusted soil samples on a vacuum line using liquid N_2. Following purification, samples were graphitized with an iron catalyst under an H_2 enriched atmosphere at 550°C. Radiocarbon content was then measured by accelerator mass spectrometry (Micadas, Ionplus, Switzerland) at the Max Planck Institute for Biogeochemisty (Steinhof, 2017).

We report radiocarbon values using units of $\Delta^{14}C$, defined as the deviation in parts per thousand of the ratio of ^{14}C–^{12}C from that of the oxalic acid standard measured in 1950. This unit also contains a correction for the potential effect of mass-dependent fractionation

by normalizing sample δ^{13}C to a common δ^{13}C value of 25 per mil (Stuiver & Polach, 1977). Values with Δ^{14}C >0 indicate the presence of "bomb" C produced by atmospheric weapons testing in the early 1960s. Values with Δ^{14}C < 0 indicate the influence of radioactive decay of ^{14}C, which has a half-life 5730 years.

Statistical analysis

We used a linear modeling approach to assess the relative explanatory power of climate versus parent material on the observed variation in Δ^{14}C, as well as potential interactions between these two factors. We constructed separate models for $\Delta^{14}C_{bulk}$ and $\Delta^{14}C_{respired}$ but with the same righthand side of the equation (**Eq. 1**). For each model we considered the two-way interaction between parent material and climate as well as the three-way interaction with time (**Eq. 1**). For ease of interpretation, we considered the effect of depth by modeling each depth layer separately (0-10 cm, 10-20 cm, 20-30 cm). We also made pairwise comparisons of $\Delta^{14}C_{bulk}$ and $\Delta^{14}C_{respired}$ across sites and within years, as well as comparisons of individual sites across years. We assessed the significance of the temporal trend for pairwise combinations of parent material and climate using the emmtrends function of the emmeans package (Lenth, 2021). We corrected for multiple comparisons using Tukey's honestly significant mean difference.

Eq. 1

$$\Delta^{14}C = \alpha + \beta_1(Parent\_material) \times \beta_2(Climate) \times \beta_3(Year) + \epsilon$$

The relationship between Δ^{14}C of bulk soil and respired CO_2 provides insight into soil C dynamics and potential retention mechanisms (Sierra et al. 2018). We modeled the effects of parent material (**Eq. 2**) and climate (**Eq. 3**) on this relationship separately, as we did not have an adequate number of observations to consider the interaction between these two explanatory variables. We used Δ^{14}C measurements made on samples collected in 2001 and

2019, and data from all depths. The three-way interactions of $\Delta^{14}C_{bulk}$ and the explanatory variables were not significant with either depth or time for either **Eq. 3** or **Eq. 4**, so we did not include those variables in the models.

Eq. 2

$$\Delta^{14}C_{respired} = \alpha + \beta_1(\Delta^{14}C_{bulk}) \times \beta_2(Parent\_material) + \epsilon$$

Eq. 3

$$\Delta^{14}C_{respired} = \alpha + \beta_1(\Delta^{14}C_{bulk}) \times \beta_2(Climate) + \epsilon$$

We assessed the relative importance of poorly crystalline versus crystalline iron minerals in protecting soil C from microbial decomposition by regressing $\Delta^{14}C$ against the concentrations of ammonium-oxalate extractable iron, ammonium-oxalate extractable aluminum, pyrophosphate extractable aluminum, and dithionite-citrate extractable iron (**Eq. 4**). We fit the model for $\Delta^{14}C_{bulk}$, $\Delta^{14}C_{respired}$, and the difference between $\Delta^{14}C_{respired}$ and $\Delta^{14}C_{bulk}$ ($\Delta^{14}C_{bulk\text{-}respired}$). We used $\Delta^{14}C$ data from 2001 and 2019. Selective dissolution was only performed for the soils collected in 2001, as these data reflect weathering processes that operate timescales beyond the 18 year duration of this study. Extracted metal concentrations did not change substantially by horizon; therefore we conducted regressions for the entire 0-30 cm depth in order to control for the depth dependence of $\Delta^{14}C$ and simplify interpretation of the data. We computed carbon mass-weighted means for $\Delta^{14}C_{bulk}$ data and flux-weighted means for $\Delta^{14}C_{respired}$ data prior to calculating $\Delta^{14}C_{bulk\text{-}respired}$.

Eq. 4

$$\Delta^{14}C = \alpha + \beta_1(Metal_x) + \beta_2(time) + \epsilon$$

Results

Soil carbon concentration depth profiles

We observed both parent material and climate effects on soil carbon concentrations. Carbon concentrations were similar among parent materials for the warm climate sites (**Fig. 1, a)**), while at the cool and cold climate sites (**Fig. 1, b, c**) the andesitic soils had higher concentrations than either the basaltic or granitic soils. The basaltic and granitic soils had similar carbon concentrations across climate zones, while the cool and cold climate andesitic soils were enriched in carbon relative to the warm climate soils. Soils showed a similar decrease in carbon concentration with depth across all sites (**Fig. 1**).

We did not observe significant changes in soil carbon concentration over time at the majority of sites. However, there were a few exceptions. Most notably, we saw significant increases in soil C concentration for the cold climate andesitic soils at all depths (lower and upper 95% confidence limits given in bracks): 0.20 [0.01, 0.40], 0.23 [0.12, 0.35], 0.21 [0.13, 0.29] increase in percent C yr^{-1}, for the 0-10, 10-20, and 20-30 cm depth increments, respectively. We also saw a significant increase in percent C over time for the 10-20cm layer at the warm climate granitic site (0.16 [0.05, 0.26]), and significant decreases for the 0-10cm layer at the warm climate andesitic and basaltic sites (-0.19 [-0.37, -0.01], 0.04 [-0.07, 0.14]).

Radiocarbon depth profiles

Bulk soil. We observed the most enriched $\Delta^{14}C_{bulk}$ at the warm climate sites (**Fig. 2, a**). Contrary to what would be expected from the decomposition-temperature relationship, however, $\Delta^{14}C_{bulk}$ of soils at the cool climate sites was equally or more depleted than what we observed at the cold climate sites (**Fig. 2, b, c**). When comparing parent materials within climate zones, $\Delta^{14}C_{bulk}$ of andesitic soils tended to be the most depleted,

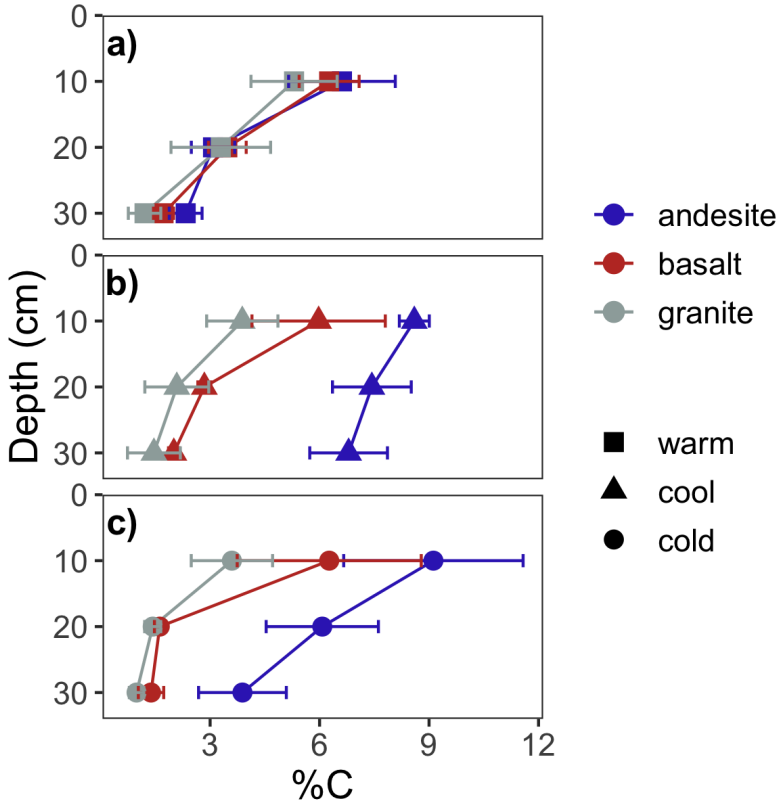

Figure 1. Profiles of soil C concentration. Points show means of samples collected in 2001, 2009, and 2019; error bars show ±2 standard errors.

while the granitic soils tended to be the most enriched (**Fig. 2**).

Analysis of variance for $\Delta^{14}C_{bulk}$ revealed significant two-way interactions between parent material and climate at all depths (**Table 1**). Accordingly, we observed greater differences in $\Delta^{14}C_{bulk}$ among parent materials at the warm and cool sites (**Fig. 2, a, b**) than at the coldest sites (**Fig. 2, c**). Although $\Delta^{14}C_{bulk}$ declined with depth for all sites, climate explained more of the variance for the uppermost soil layer (0-10 cm) whereas parent material explained more in the bottom two layers (10-20 cm, 20-30 cm) (**Table 1**).

Heterotrophically respired CO_2. The patterns we observed for $\Delta^{14}C_{respired}$ were similar to what we observed for $\Delta^{14}C_{bulk}$ (**Fig. 2**). We found climate to be the most significant factor for explaining the variance observed in $\Delta^{14}C_{respired}$ for the uppermost soil

layer, as with $\Delta^{14}C_{bulk}$, but unlike $\Delta^{14}C_{bulk}$, parent material was not significant for explaining the variance in $\Delta^{14}C_{respired}$ at this depth (**Table 2**). However, at the deepest depth, we found parent material to be more important than climate for explaining in $\Delta^{14}C_{respired}$ variance (**Table 2**). Overall, the interaction between parent material and climate explained more of the variance in $\Delta^{14}C_{respired}$ data than in the $\Delta^{14}C_{bulk}$ data (**Table 2**).

We observed that the effect of climate on $\Delta^{14}C_{respired}$ was moderated by the effect of parent material. For the andesitic soils there were no significant differences in $\Delta^{14}C_{respired}$ when compared across climate zones at any depth (SI Table X Tukey results for emm?). In contrast, $\Delta^{14}C_{respired}$ for the basaltic and granitic soils diverged substantially between climate zones, particularly for the 10-20 cm and 20-30 cm depth layers (**Fig. 2**). Overall, $\Delta^{14}C_{respired}$ across sites was most similar at the soil surface, and most divergent at the intermediate depth (10-20 cm) (**Fig. 2**).

Radiocarbon timeseries

Table 1

ANOVA: Bulk soil

Depth	Predictor	*df*	Sum of squares	Mean square	*F*	*p*
0-10cm	Parent material	2	15060	7530	9.64	< .001
	Climate	2	29114	14557	18.63	< .001
	Year	1	19413	19413	24.85	< .001
	Parent material:Climate	4	10524	2631	3.37	.017
	Parent material:Year	2	2797	1399	1.79	.179
	Climate:Year	2	6093	3046	3.90	.028
	Parent material:Climate:Year	4	9828	2457	3.15	.023
	Residuals	44	34372	781		

Table 1

ANOVA: Bulk soil (continued)

Depth	Predictor	*df*	Sum of squares	Mean square	*F*	*p*
10-20cm	Parent material	2	34449	17224	25.26	< .001
	Climate	2	24465	12233	17.94	< .001
	Year	1	3422	3422	5.02	.030
	Parent material:Climate	4	14908	3727	5.47	.001
	Parent material:Year	2	848	424	0.62	.542
	Climate:Year	2	4102	2051	3.01	.060
	Parent material:Climate:Year	4	9237	2309	3.39	.017
	Residuals	44	30006	682		
20-30cm	Parent material	2	27434	13717	20.25	< .001
	Climate	2	14455	7228	10.67	< .001
	Year	1	2841	2841	4.19	.047
	Parent material:Climate	4	7430	1858	2.74	.040
	Parent material:Year	2	4405	2203	3.25	.048
	Climate:Year	2	13152	6576	9.71	< .001
	Parent material:Climate:Year	4	7322	1831	2.70	.043
	Residuals	44	29806	677		

Table 2

ANOVA: Heterotrophic respiration

Depth	Predictor	*df*	Sum of squares	Mean square	*F*	*p*
0-10cm	Parent material	2	242	121	0.49	.622

Table 2

ANOVA: Heterotrophic respiration (continued)

Depth	Predictor	*df*	Sum of squares	Mean square	*F*	*p*
	Climate	2	9092	4546	18.34	< .001
	Year	1	28816	28816	116.25	< .001
	Parent material:Climate	4	12294	3074	12.40	< .001
	Parent material:Year	2	385	192	0.78	.475
	Climate:Year	2	2558	1279	5.16	.017
	Parent material:Climate:Year	4	5930	1483	5.98	.003
	Residuals	18	4462	248		
10-20cm	Parent material	2	9874	4937	19.08	< .001
	Climate	2	6768	3384	13.08	< .001
	Year	1	9203	9203	35.57	< .001
	Parent material:Climate	4	26135	6534	25.25	< .001
	Parent material:Year	2	5591	2795	10.80	.001
	Climate:Year	2	6144	3072	11.87	.001
	Parent material:Climate:Year	4	8375	2094	8.09	.001
	Residuals	16	4140	259		
20-30cm	Parent material	2	13961	6981	7.06	.006
	Climate	2	4016	2008	2.03	.164
	Year	1	175	175	0.18	.680
	Parent material:Climate	4	28563	7141	7.22	.002
	Parent material:Year	2	21958	10979	11.10	.001
	Climate:Year	2	15562	7781	7.87	.004
	Parent material:Climate:Year	4	9420	2355	2.38	.095
	Residuals	16	15824	989		

Bulk soil. We observed a significant three-way interaction between parent material, climate, and time at all three depths in the linear models (**Eq. 1**) for $\Delta^{14}C_{bulk}$ (**Table 1**).

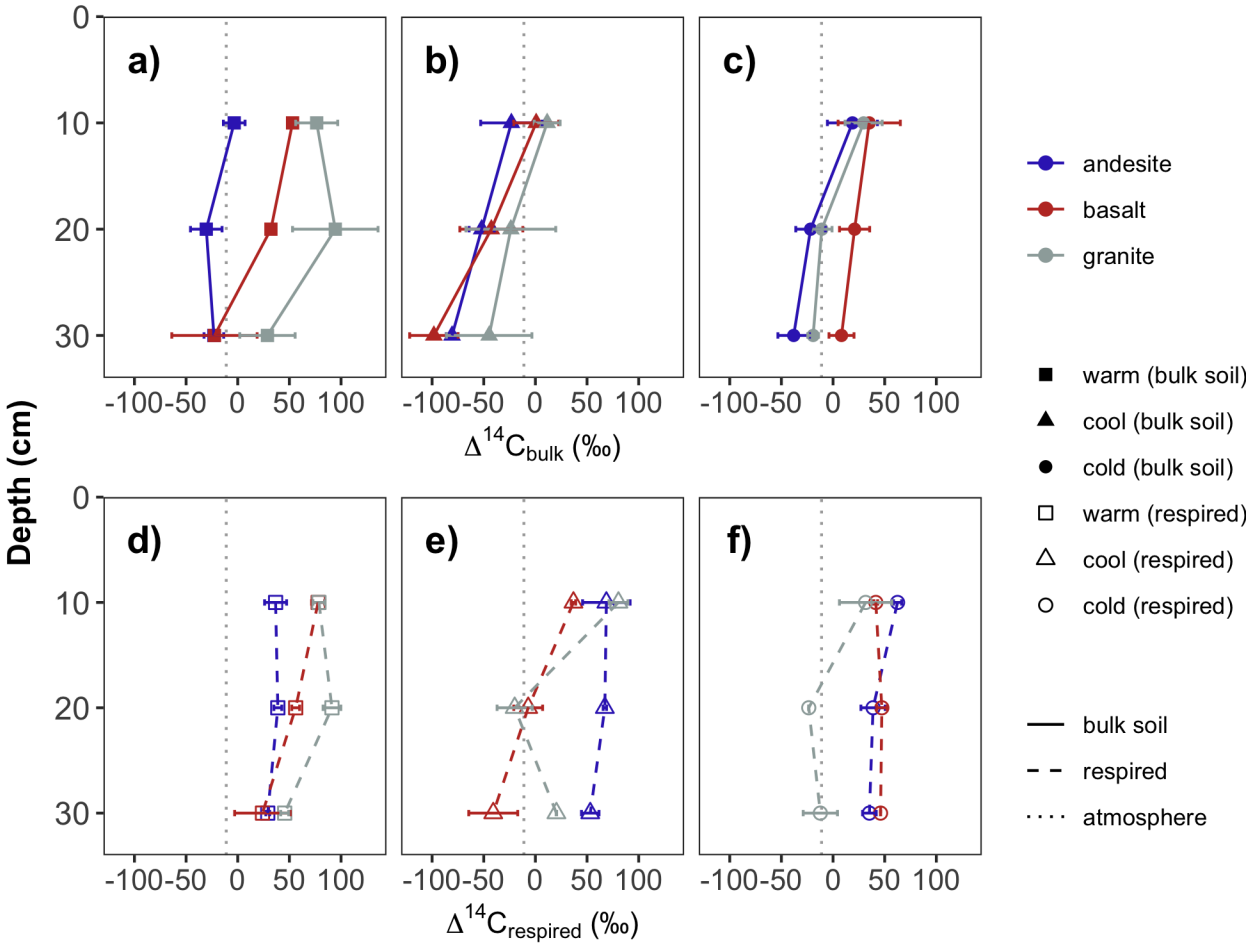

Figure 2. Depth profiles of $\Delta^{14}C_{bulk}$ and $\Delta^{14}C_{respired}$. Top panels show bulk data from 2001, bottom panels show respired data. Panels (a) and (d) show data from the warm climate sites, (b) and (e) from the cool climate sites, and (c) and (f) from the cold climate sites. Black vertical lines show $\Delta^{14}C$ of the atmosphere in the year of sampling. Points show the mean of three replicate profiles for bulk soil, and the mean of laboratory duplicates for respired CO_2. Error bars show ± 1 SD for bulk soils and the minimum and maximum for respired CO_2.

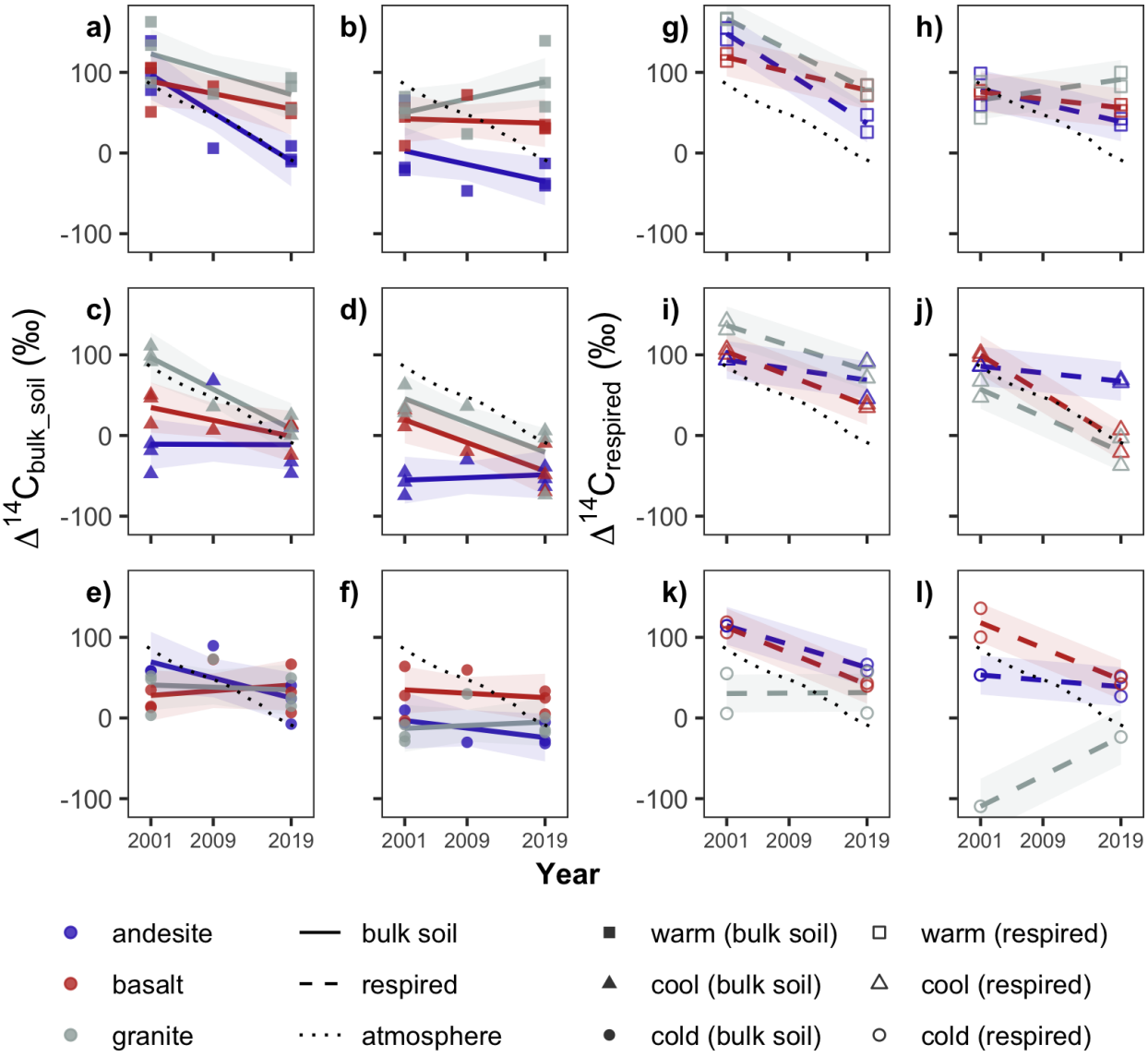

Figure 3. Temporal trends in $\Delta^{14}C$ for 0-10 cm and 10-20 cm depth layers. Panels a-f show $\Delta^{14}C_{bulk}$ data; from left, the first column (panels a, c, and e) show 0-10 cm data, and the second column (panels b, d, and f) shows 10-20 cm data. Panels g-l show $\Delta^{14}C_{respired}$ data; the third column from left (panels g, i, k) shows 0-10 cm data, and the rightmost column (panels h, j, and l) shows 10-20 cm data. Points show observed data; lines show linear trend estimates for marginal means; ribbons show 95% confidence intervals for trends. Dotted line shows atmospheric $\Delta^{14}C$.

The change over time in $\Delta^{14}C_{bulk}$ was also affected by depth, with greater differences between 2001 and 2019 seen in the uppermost soil layer than in the deeper layers (**Fig. 3**). We observed a significant decrease in $\Delta^{14}C_{bulk}$ in both warm and cool climate granitic soils for the uppermost soil layer, and additionally for the warm climate andesitic soils (**Fig. 3, a**). In the deeper soil layers (10-20 cm and 20-30 cm), we only observed a significant change over time in $\Delta^{14}C_{bulk}$ in the cool climate basalt and granite soils (**Fig. 3, b, c**). $\Delta^{14}C_{bulk}$ of the cool climate andesitic soils remained essentially unchanged between 2001 and 2019 for all depths (**Fig. 3, a, b, c**), underscoring the importance of the interaction between parent material and climate for explaining temporal trends in $\Delta^{14}C_{bulk}$ as well as variance in a given year.

The relationship of $\Delta^{14}C_{bulk}$ to atmospheric $\Delta^{14}C$ appeared to be a function of both parent material and climate. In 2001, the warm climate sites were the only sites where the basaltic and andesitic soils were enriched relative to the atmosphere, and this enrichment was only observed for the uppermost soil layer (**Fig. 3)**). In contrast, granitic soils at both the warm and cool granitic sites were enriched relative to the atmosphere in 2001 (**Fig. 3**). For the cold climate sites, where $\Delta^{14}C_{bulk}$ was most similar, all three lithologies were depleted relative to atmospheric in both surface and subsoil layers (**Fig. 3**).

We observed that $\Delta^{14}C_{bulk}$ tended to decrease or remain unchanged between 2001 and 2019 across sites, but the rates of change in $\Delta^{14}C_{bulk}$ were typically smaller than the corresponding change in atmospheric $\Delta^{14}C$ over the same period (-5.13 per mille yr^{-1}). Accordingly, $\Delta^{14}C_{bulk}$ measured in 2019 tended to be enriched relative to the atmosphere at more sites, and also deeper into the soil than in 2001. We observed surface soil $\Delta^{14}C_{bulk}$ (0-10 cm) in 2019 to be enriched relative to the atmosphere at all sites except for the cool climate andesite soils (**Fig. 3; Fig. 2, d-f**). Furthermore, $\Delta^{14}C_{bulk}$ remained enriched relative to the atmosphere down to 30 cm at two of the sites in 2019: the warm climate granite soil (**Fig. 2, d**) and cold climate basalt soil (**Fig. 2, f**). $\Delta^{14}C_{bulk}$ at the cool

andesite site was the most depleted relative to the atmosphere at all time points (**Fig. 3**).

Heterotrophically respired CO_2. Temporal trends in $\Delta^{14}C_{respired}$ were similar to what we observed for $\Delta^{14}C_{bulk}$, but tended to be of greater magnitude (**Fig. 3, g-l**). Although greater than the change over time we observed in $\Delta^{14}C_{bulk}$, changes in $\Delta^{14}C_{respired}$ between 2001 and 2019 still tended to be smaller in magnitude than the change observed in the atmosphere over this period (**Fig. 3, g-l**). In contrast to $\Delta^{14}C_{bulk}$, $\Delta^{14}C_{respired}$ tended to be indistinguishable or enriched relative to the atmosphere in both 2001 and 2019; while the majority of samples were enriched relative to the atmosphere in 2019, even at depth (**Fig. 3, g-l**).

We saw significant decreases in surface soil $\Delta^{14}C_{respired}$ at seven of the nine sites, with the only exceptions being the cool andesitic and cold granitic sites (**Fig. 3, i, k**). In absolute terms, the changes in $\Delta^{14}C_{respired}$ over time in these uppermost soil layers were greatest at the warm sites (-4.43835320190356 per mil $\pm$1.99225321446124 yr^{-1}), while changes were similar for the cool and cold sites (-2.73813429537826 per mil $\pm$1.20546613003229 yr^{-1}, and -2.25428740225863 per mil $\pm$2.07929272876693 yr^{-1}, respectively). The magnitude of the change in $\Delta^{14}C_{respired}$ over time tended to decrease with depth. We observed significant negative trends over time for $\Delta^{14}C_{respired}$ at only four of the nine sites for the 10-20 cm layer (warm andesite, cool basalt, cool granite, and cold basalt) (**Fig. 3**), and only one site for the 20-30 cm layer (cold basalt) (SI). $\Delta^{14}C_{respired}$ at the cool andesitic soils remained unchanged at all depths over the study period.

We observed a significant increase in $\Delta^{14}C_{respired}$ from 2001 to 2019 at only one site: from the cold climate granitic soils (**Fig. @ref(fig:plot-ts-14c**). These were also the only soils for which $\Delta^{14}C_{respired}$ was more depleted than $\Delta^{14}C_{bulk}$. We observed this anomaly for the deeper soil layers in both 2001 and 2019. For the 8-27 cm layer in 2001, the range of $\Delta^{14}C_{respired}$ values was -469.10 and -127.80 per mil, compared to a range of $\Delta^{14}C_{bulk}$ values of -30.80 and -10.50; similarly, for the 10-20 cm layer in 2019 we observed a range of $\Delta^{14}C_{respired}$

values of -396.70 and -23.50 per mil compared to -18.10 and 0.40 for $\Delta^{14}C_{bulk}$ (SI Table X). We do not believe this was due to laboratory error in spite of the high variance we observed in the samples, as the pattern was restricted to the deeper soil layers from this one site and consistent over time. However, since it appears to be a unique response to these soils, we have excluded these highly depleted samples from the statistical analyses.

Relationship of bulk soil and respired CO_2 $\Delta^{14}C$

We also assessed whether interaction effects of parent material or climate with $\Delta^{14}C_{bulk}$ led to deviations from a 1:1 relationship with $\Delta^{14}C_{respired}$ (**Fig. 4**). We found that changes in $\Delta^{14}C_{bulk}$ led to correspondingly smaller changes in $\Delta^{14}C_{respired}$ for andesitic soils in the parent material only model (**Eq. 2**) (slope = 0.51, 95% CI = [0.22, 0.80]) (**Fig. 4, a**), and for cool climate soils in the climate only model (**Eq. 3**) (slope = 0.61, 95% CI = [0.30, 0.91]) (**Fig. 4, b**). While we could not directly test the interaction of parent material and climate factors in these models owing to the limited number of observations, mean differences in $\Delta^{14}C_{bulk}$ and $\Delta^{14}C_{respired}$ were substantially greater for the cool climate soils developed on andesitic parent material than for the other sites (Table? Numbers?).

Mineral assemblages and radiocarbon

Mineral assemblage data is reported fully in Rasmussen et al. (2018). Here we focus on the selective dissolution data with respect to the trends we observed in $\Delta^{14}C_{bulk}$, $\Delta^{14}C_{respired}$, and $\Delta^{14}C_{respired\text{-}bulk}$. We observed a significant negative correlation between $\Delta^{14}C_{bulk}$ and the concentration of oxalate extractable iron, oxalate extractable aluminum, and pyrophosphate extractable aluminum (SI). For simplicity, we focus here on the sum of oxalate extractable aluminum and half of the oxalate extractable iron as a proxy for poorly crystalline mineral abundance, and the difference of dithionite-citrate extractable iron and ammonium-oxalate

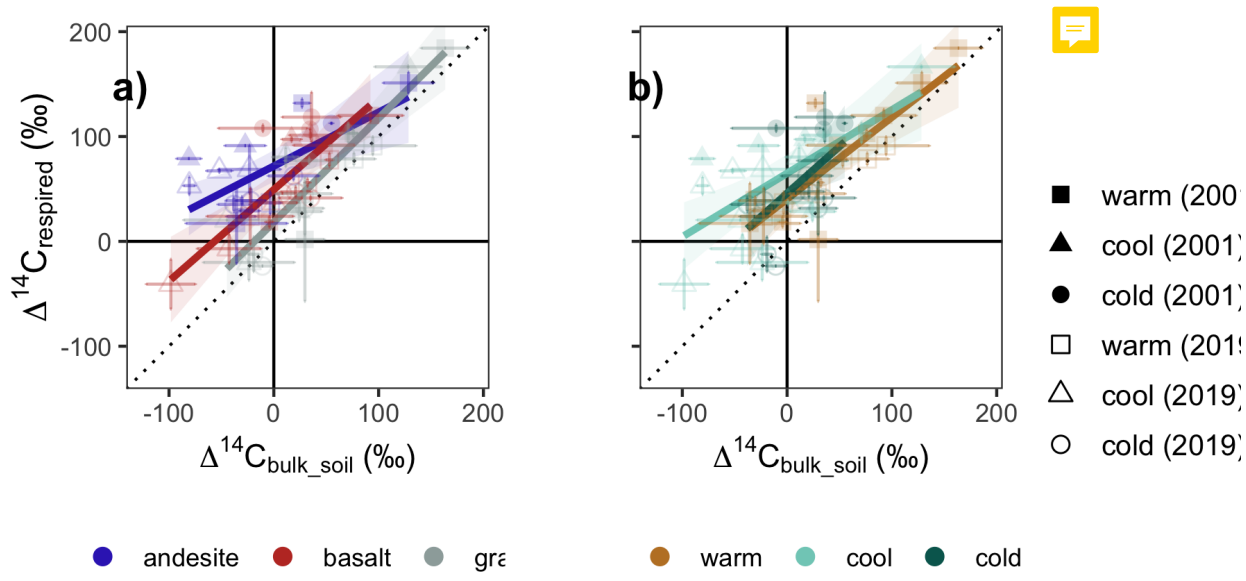

Figure 4. Parent material and climate effects on the relationship of $\Delta^{14}C_{bulk}$ and $\Delta^{14}C_{respired}$. [a)] Parent material model **(Eq. 3)** and [b)] Climate model **(Eq. 4)**. Dotted line shows 1:1 relationship. Points show the mean of three replicate profiles for bulk soil, and the mean of laboratory duplicates for respired CO_2. Error bars show ±1 SD for bulk soils and the minimum and maximum for respired CO_2. Respired CO_2 from the cold granite site in 2001 was extremely depleted in $\Delta^{14}C$ and thus is excluded for display purposes.

extractable iron as a proxy for crystalline mineral abundance. The relationship between non-crystalline mineral abundance and $\Delta^{14}C_{bulk}$ was highly significant (p <0.001), with the model explaining 59 percent of the observed variation. In contrast, we did not find a significant relationship between crystalline mineral abundance and $\Delta^{14}C_{bulk}$.

We also observed a significant ($p = 0.02$) negative relationship between $\Delta^{14}C_{respired}$ and non-crystalline mineral abundance, although it was not as strong as the $\Delta^{14}C_{bulk}$ relationship. However, we observed a stronger relationship between poorly crystalline mineral abundance and $\Delta^{14}C_{respired\text{-}bulk}$ than for either $\Delta^{14}C_{bulk}$ or $\Delta^{14}C_{respired}$ (**Fig.**

303 **@ref(fig:blk-inc-plots, b)**. As with $\Delta^{14}C_{bulk}$, there was no relationship with crystalline
304 mineral abundance for either $\Delta^{14}C_{bulk}$ or $\Delta^{14}C_{respired\text{-}bulk}$ (**Fig. @ref(fig:blk-inc-plots, b)**.

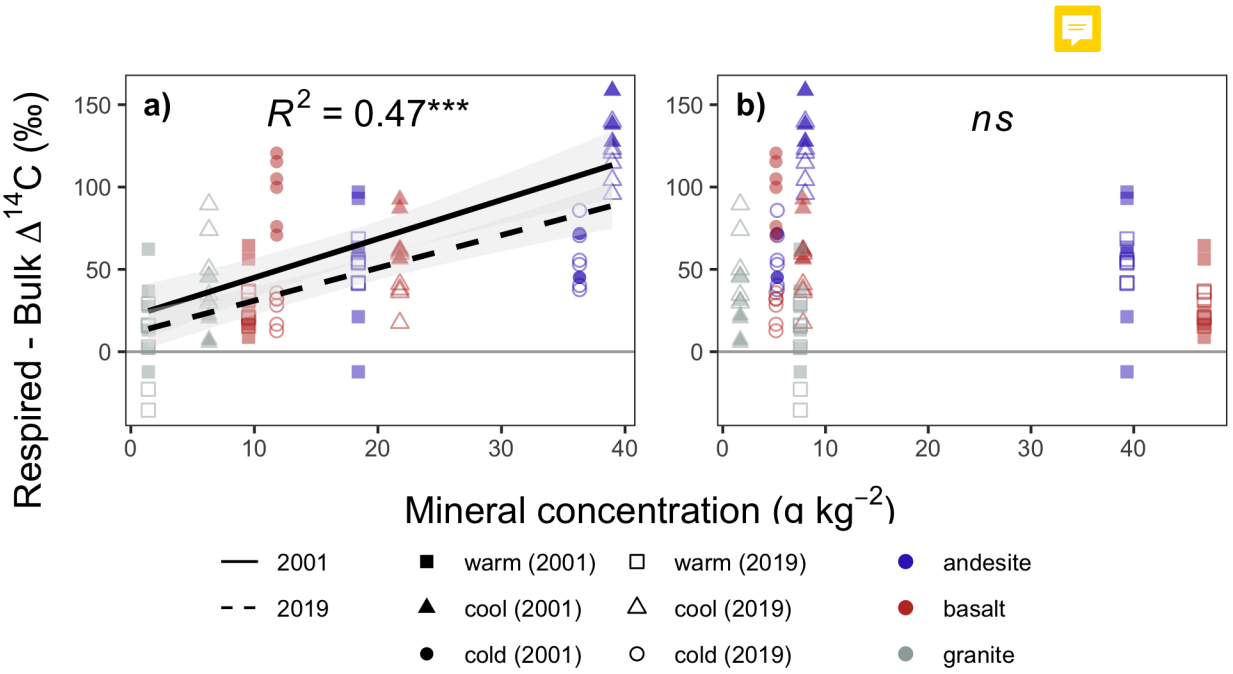

Figure 5. Relationship of poorly crystalline and crystalline minerals to the difference of $\Delta^{14}C_{respired}$ and $\Delta^{14}C_{bulk}$ ($\Delta^{14}C_{respired\text{-}bulk}$). [a)] Poorly crystalline mineral content (oxalate-extractable aluminum + 1/2 oxalate-extractable iron), [b)] Crystalline mineral content (dithionite-extractable iron - oxalate-extractable iron). Points show mass-weighted mineral concentrations and carbon-weighted values of $\Delta^{14}C_{respired\text{-}bulk}$ for 0-30cm profiles. Lines show linear model fits from **Eq. 5**.